Simulations of Gas-Liquid-Solid 3-Phase Flow and Reaction in FCC Riser Reactors

Jinsen Gao, Chunming Xu, Shixiong Lin, and Guanghua Yang
State Key Laboratory of Heavy Oil Processing, University of Petroleum, Beijing, 102200, P.R. China

Yincheng Guo
Dept. of Engineering Mechanics, Tsinghua University, Beijing, 100084, P.R. China

A 3-D, three-phase flow-reaction model was developed to predict the performance of FCC riser reactors. This model incorporates the effect of feed vaporization into an earlier 3-D, two-phase flow-reaction model (Gao et al., 1999). The synergistic effects of hydrodynamics, heat transfer, and feed vaporization on FCC reactions are elucidated. The results show that a complex phenomenon occurs in the zone up to 4m above the point at the bottom of the riser reactor where feed is injected. The changes in the spray droplet diameter, volumetric concentration and temperature of the feed in the feed injection zone are illustrated. The model was used as a design tool for an operation modification study. Results indicate that FCC reaction selectivity for the desired products (gasoline and light fuel oil) can be improved by reducing initial droplet diameter in the feed spray from 80 to 40 μm.

Introduction

In modern petroleum refineries, the fluid catalytic cracking (FCC) unit is the key process for the profitable conversion of heavy petroleum fractions into lower molecular-weight products, such as gasoline and light olefins. FCC technology has continued to evolve since its advent nearly half a century ago. During this time, many improvements have been made in FCC operation; these include feed preparation, catalyst development, equipment design, and operating strategies.

In addition, a more comprehensive understanding of the relevant technologies, particularly fluidization, has brought about major changes. The catalytic cracking reaction is initiated and completed in short-contact-time riser reactors in which the catalyst is pneumatically conveyed from the bottom to the top by steam and hydrocarbon vapors. During the conveying process the efficient mixing and contact of catalyst with hydrocarbons enhances the catalytic cracking reactions. Although the FCC process comprises two key units, namely a reactor and a regenerator, the development of more active molecular sieve cracking catalysts in the 1970s has led to the riser reactor becoming the dominant process component (Chen and Cao, 1995). It is necessary to point out that gas–solid riser reactors have been widely utilized as well in other chemical processes.

Based on the advantage of riser reactors, riser cracking is established as today's reaction system of preferred choice. The process in a riser reactor is typically turbulent, multiphase flow with reaction, and comprises many complex subprocesses, such as: catalytic cracking, momentum transfer, heat transfer, and mass transfer, all of which are known to be interrelated (Chen, 1985). A thorough review of the research and development related to FCC riser reactors can be divided into three categories, as follows (Gao et al. 1999):

- Catalytic cracking kinetics models, assuming isothermal plug-flow of the riser reactor
- Cold-flow two-phase turbulent hydrodynamics in risers
- Complex feed vaporization phenomena in the feed-injecting zone.

Preheated heavy-oil feed is injected onto hot regenerated catalysts in the feed-injection zone of the FCC riser. About 5 wt % steam that serves as atomizing media is injected into

Correspondence concerning this article should be addressed to J. Gao.

the feed-injection zone as well, together with the preheated heavy oil feed. For a typical feed injector design the catalyst, flowing up at high density, comes into contact with feed from a high-penetration introduction system. Catalyst particles are coated with a thin film of oil and simultaneously cooled as they flow through the feed spray. Meanwhile, the feed spray vaporizes rapidly owing to close contact with the hot catalyst particles. The increased amount of vapor, from the reaction and vaporization, including atomizing steam, raises the velocity and lowers the density of the flowing system (Murphy, 1992).

The initial process occurring at the bottom of the riser reactor becomes the important step in determining unit performance, even dominating the product distribution and quality (Mauleon and Courcelle, 1985; Xie, 1985; Mo et al, 1991a,b; Murphy, 1992). These authors considered the effects of feed atomization, feed spray pattern, the condition of feed oil spray drops contacting regenerated catalyst particles, and feed spray vaporization. Partial feed vaporization leads to a three-phase flow (catalyst, liquid hydrocarbons, hydrocarbon vapor, and steam) at the entrance region of the feed-injection zone of the FCC riser and for about 3 ~ 4 m in the riser. As the mixture moves along the riser, complete feed vaporization results in a two-phase flow (catalyst, hydrocarbon vapor and steam) that begins at about 3 ~ 4 m of the riser height.

The effects of feed vaporization and feed-injection configuration have been evaluated in experimental studies in commercial catalytic cracking reactors and pilot units. Mauleon and Courcelle (1985) showed that the interphase heat transfer and feed-spray atomization have major impacts on feed vaporization, in turn affecting the temperature and concentration distributions. Feed-injector geometry affects system hydrodynamics and further influences heat balance and reaction kinetics.

Mo et al. (1991a,b) carried out a comprehensive study on the initial dynamic process, using a downflow pilot riser unit. They determined the effect on cracking reactions using Daqing atmospheric residuum as feed. Their pilot riser unit was equipped with separate zones to allow examination of both partial feed-spray vaporization and contact of vaporized and unvaporized spray with hot regenerated catalyst in an oil–catalyst mixing zone. Different spray droplet diameters and size distribution were obtained by varying the operating parameters and design of the feed nozzle. The history of feed-spray vaporization, including its motion, its age distribution, and its vaporization rate were determined. Effects of the initial dynamics process at the beginning of catalytic cracking on the cracking reaction were consequently obtained. It was concluded that good feed atomization is essential for best product yield. Although the riser reactor used was somewhat different to a commercial unit, this study revealed the importance of feed vaporization effects.

Schuurmans (1980) conducted a series of tests with a modern catalytic cracking unit in which feed was injected into the catalyst stream through three separate nozzles uniformly spaced around the circumference of the riser. From helium trace studies, Schuurmans (1980) concluded that the feed-catalyst mixing was poor at the bottom of the reactor. A typical vapor-phase conversion profile along the riser height was also measured, indicating a local conversion minimum at the bottom of the reactor. This minimum vapor-phase conversion was explained by assuming that the low vaporization rates and hydrocarbon adsorption on the catalyst surfaces were related to imperfect mixing of feed and catalyst.

Research by Dean et al. (1982) showed that the heat-transfer rate between feed-spray droplets and catalyst particles varied exponentially with feed-spray diameters, indicating that this parameter is most important with regard to vaporization rate. The smaller the feed-spray diameters, the faster the feed-spray evaporation rate, leading to a better mixing with catalyst and more uniform cooling of catalyst particles with a concomitant reduction in undesired thermal cracking.

In recent years, a tremendous effort has been made to develop simulation models, incorporating FCC reaction kinetics and complex hydrodynamics in a single model. Theologos and Markatos (1993) developed a computational fluid dynamics (CFD) model to assess changes in operating parameters on FCC riser reactions, including the impact of feed-injector geometry on hydrodynamics, particularly near the bottom of the reactor. Gao et al. (1999) extended this work and developed a 3-D, two-phase turbulent flow-reaction model. These authors incorporated a modified two-phase turbulent model for the comparatively dense particle phase with interphase heat transfer and thirteen-lump reaction kinetics for residuum cracking. The model can be used as a design tool for operational case studies and to predict the performance of FCC riser reactors.

Although the model derived by Gao et al. (1999) has proven satisfactory for process simulation in the FCC riser, it lacks the flexibility to account for the effect of feed spraying. This model was based on the premise of instant feed vaporization as it enters the riser reactor. This is an oversimplified assumption owing to the limited interphase heat transfer between catalyst particles and feed-oil spray droplets, especially for residuum FCC feed (Xu et al., 1997).

Theologos et al. (1997) developed an integrated CFD model with 10-lump reaction kinetics, which incorporated the feed-spray vaporization effect. This model is important in FCC feed nozzle design and operation. They assumed that feed-spray vaporization occurs in a single-phase (gas-phase) regime and only modified the heat-transfer equations for gas and solid phases. To provide better descriptions of the hydrodynamics, temperature profile and vaporization of feed-spray droplets inside the riser reactor, further improvements are needed.

In this study, a 3-D, gas–liquid–solid three-phase flow-reaction model was developed by extending the 3-D, two-phase turbulent flow-reaction model (Gao et al., 1999). The feed vaporization inside the riser reactor is modeled with a set of governing equations for the feed-spray droplets. Model predictions are compared with the performance data from commercial riser reactors. A process study on the effect of feed-spray droplet size is also discussed.

Model Description

A general overview of the two-phase flow and reaction model derivation for the FCC riser reactor has been described by Gao et al. (1999). The focus of the work presented here is the vaporization of feed-spray. The velocity of FCC feed through the nozzle in a typical commercial riser varies from 50 m/s to 60 m/s, falling to 10 to 20 m/s in the reactor

itself. The vaporization of feed, containing a portion of vacuum residuum, can be completed within 0.2 s if the feed-spray droplets are 60 μm (Liu and Han, 1992); this value can be achieved with typical commercial FCC nozzles.

It can be determined that the feed spray will survive inside the riser for a distance of 2–4 m from the inlet. In other words, feed-spray exists in an area close to the feed-injection zone where vaporization of the surviving feed spray and cracking reactions of the vaporized hydrocarbon feed take place simultaneously. Catalyst particles supply the endothermic heat needed for vaporization and cracking reactions. In reality, feed vapors, unvaporized feed-spray, and catalysts coexist in the feed-injection zone as a gas–liquid–solid three-phase flow regime. In the most complex process in a riser reactor, large amounts of endothermic heat for feed vaporization and cracking reactions causes nonuniformity of both temperature and concentration distribution in the three phases.

To better depict the complex process of feed-spray flow and vaporization inside the riser reactors, the feed-spray droplets were considered as a separate phase in addition to the gaseous and catalyst particle phases. A separate set of governing equations describing the feed-spray droplet flow, heat absorption, and vaporization, and their interaction with the gaseous and catalyst particle phases were developed. By solving the governing equations, the gas–liquid–solid three-phase flow along the riser reactor can be visualized. Most importantly impacts of process parameters on the FCC riser reactor can be assessed.

A complete physical model of gas–liquid–solid three-phase flow and reactions in FCC riser reactors should include all of the components shown on Figure 1. This physical model shows many complex couplings and correlations of the turbulent flow, heat transfer, mass transfer, and catalytic cracking reactions among the gaseous, feed-spray droplet and catalyst particle phases. As for the feed-spray, one has to consider flow behavior, heat transfer, and vaporization, as well as synergetic effects with the gaseous and catalyst particle phases. In essence, the development of the gas–liquid–solid three-phase flow-reaction model for an FCC riser reactor is to quantify the flow-reaction characteristics of three phases and their complex coupling relationships.

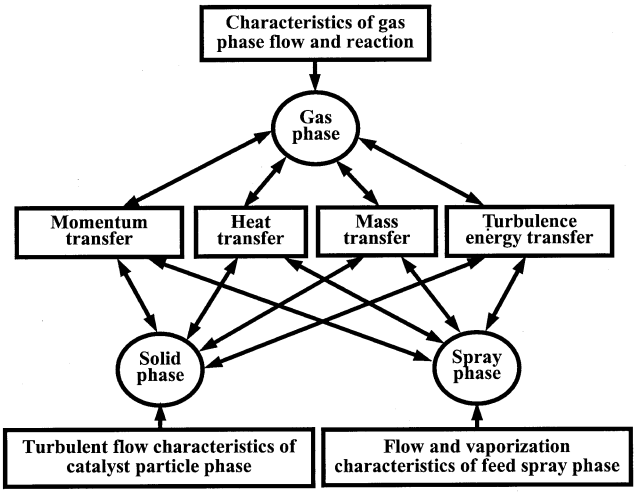

Figure 1. Physical model of gas–liquid–solid three-phase flow and reaction in FCC riser reactors.

Governing equations

The gas–liquid–solid three-phase flow-reaction model was based on the Eulerian multifluid approach (Guo, 1995), in which gaseous phase, feed-spray droplet phase, and catalyst particle phase are considered as a continuum. It was assumed that complete vaporization of the feed occurs in the riser. Both vaporizing rate and temperature are assumed to be constant. The governing equations of the three-phase flow-reaction model for mass, momentum, heat, and species in an FCC riser reactor can be expressed in the following forms.

For the gas phase:

$$\frac{\partial}{\partial t}(\epsilon_g \rho_g) + \frac{\partial}{\partial x_j}(\epsilon_g \rho_g v_j) = n_k \dot{m}_k \tag{1}$$

$$\frac{\partial}{\partial t}(\epsilon_g \rho_g v_i) + \frac{\partial}{\partial x_j}(\epsilon_g \rho_g v_j v_i) = - \epsilon_g \frac{\partial P}{\partial x_i} + \frac{\partial}{\partial x_j}\left[\mu\left(\frac{\partial v_j}{\partial x_i} + \frac{\partial v_i}{\partial x_j}\right)\right] + \epsilon_g \rho_g g_i + \frac{\rho_p}{\tau_{rp}}(v_{pi} - v_i) + \frac{\rho_k}{\tau_{rk}}(v_{ki} - v_i) + v_i n_k \dot{m}_k \tag{2}$$

$$\frac{\partial}{\partial t}(\epsilon_g \rho_g C_p T) + \frac{\partial}{\partial x_j}(\epsilon_g \rho_g v_j C_p T) = \frac{\partial}{\partial x_j}\left(\lambda \frac{\partial T}{\partial x_j}\right) - \sum_{S=1}^{13} W_S Q_{RS} + n_p Q_p + C_{pk} T_k n_k \dot{m}_k \tag{3}$$

$$\frac{\partial}{\partial t}(\epsilon_g \rho_g Y_s) + \frac{\partial}{\partial x_j}(\epsilon_g \rho_g v_j Y_s) = \frac{\partial}{\partial x_j}\left(\epsilon_g \rho_g D \frac{\partial Y_s}{\partial x_j}\right) + W_S + \alpha_s n_k \dot{m}_k. \tag{4}$$

For the catalyst particle phase:

$$\frac{\partial \rho_P}{\partial t} + \frac{\partial}{\partial x_j}(\rho_p v_{pj}) = 0 \tag{5}$$

$$\frac{\partial n_p}{\partial t} + \frac{\partial}{\partial x_j}(n_p v_{pj}) = 0 \tag{6}$$

$$\frac{\partial}{\partial t}(\rho_p v_{pi}) + \frac{\partial}{\partial x_j}(\rho_p v_{pj} v_{pi}) = \frac{\rho_p}{\tau_{rp}}(v_i - v_{pi}) + \rho_p g_i - \epsilon_p \frac{\partial P}{\partial x_j} + \frac{\partial}{\partial x_j}\tau_{p,ij} \tag{7}$$

$$\frac{\partial}{\partial t}(\rho_p C_{pp} T_p) + \frac{\partial}{\partial x_j}(\rho_p v_{pj} C_{pp} T_p) = - n_p Q_p - n_k Q_k. \tag{8}$$

For the feed-spray droplet phase:

$$\frac{\partial}{\partial t}\rho_k + \frac{\partial}{\partial x_j}(\rho_k v_{kj}) = -n_k \dot{m}_k \tag{9}$$

$$\frac{\partial n_k}{\partial t} + \frac{\partial}{\partial x_j}(n_k v_{kj}) = 0 \tag{10}$$

$$\frac{\partial}{\partial t}(\rho_k v_{ki}) + \frac{\partial}{\partial x_j}(\rho_k v_{kj} v_{ki}) = \frac{\rho_k}{\tau_{rk}}(v_i - v_{ki}) + \rho_k g_i - v_i n_k \dot{m}_k \tag{11}$$

$$\frac{\partial}{\partial t}(\rho_k C_{pk} T_k) + \frac{\partial}{\partial x_j}(\rho_k v_{kj} C_{pk} T_k) = n_k m_k C_{pk} \dot{T}_{kl} - C_{pk} T_k n_k \dot{m}_k, \tag{12}$$

where m_k and $\dot{m}_k$ denote the mass and the mass varying rate of a single feed-spray droplet, respectively. The latter is also the vaporization rate of feed-spray, and n_k and n_p denote number density of feed-spray droplet and catalyst particle, respectively. The rate of temperature rise is $\dot{T}_{kl}$ and the time scale characterizing the response for a single spray droplet is τ_{rk}, α_s is the mass fraction of the s component of the vaporized feed, reflecting the mass contribution of the vaporized feed to the s component of hydrocarbon vapors. After ρ_k and n_k are acquired by solving Eqs. 9 and 10, the progress of feed-spray droplet vaporization can be determined directly everywhere in the Eulerian coordinate system, but mainly at the bottom of the riser reactor, through the relationship $m_k = \rho_k/n_k$.

In Eqs. 1 to 12, some source terms with specific meanings for the three-phase flow and reaction model should be clarified. To begin, $n_k \dot{m}_k$ in Eqs. 1 and 9 shows the mass transfer from the feed-spray phase to gaseous phase, and $v_i n_k \dot{m}_k$ in Eqs. 2 and 11 represents the effect of the mass variation of the feed-spray droplet phase on the momentum of gaseous and feed-spray droplet phases. In addition, $\alpha_s n_k \dot{m}_k$ in Eq. 4 reflects the effect of the feed-spray evaporation on s species equation; $C_{pk} T_k n_k \dot{m}_k$ in Eqs. 3 and 12 represents the effect of the feed-spray evaporation on the enthalpy of gaseous and feed-spray droplet phases; $n_k m_k C_{pk} \dot{T}_{kl}$ in Eq. 12 describes the effect of the feed-spray temperature rise on its enthalpy equation; $n_k Q_k$ and $n_p Q_p$ are the heat transferred from catalyst phase to the feed-spray phase and the convection heat transfer between the gaseous phase and solid phase; $\sum_{S=1}^{13} W_S Q_{RS}$ represents the effect of endothermic cracking reactions on the heat balance of the system; and W_S presents the catalytic cracking reaction rate of the s component. Actually, catalytic cracking reactions only occur on the catalyst surface. But the concentration of the s component in the main flow, that is, the gaseous phase is used in the reaction rate, W_S, because it is hard to get the reactant concentrations on the catalyst surface. For the sake of simulation, substituting the concentration in the main flow for the surface concentration is reasonable and practical because the reactant concentration on the catalyst surface was determined by the reactant concentration in the main flow. So, W_S only appears in the gaseous species balance equations. Obviously, catalytic cracking reactions cannot take place in the feed-spray phase.

Feed vaporization exerts a large influence on heat transfer and catalytic cracking reactions. The existing 3-D, gas–liquid–solid flow-reaction model for the FCC riser was modified to reflect this by incorporating the variables, just described, into the basic conservation equations.

The Reynolds-averaging approach was used on the instantaneous governing equations listed previously to obtain the basic conservation equations for the turbulent flow and reaction regime inside an FCC reactor. The Reynolds-averaging procedure divided a conserved scalar value ϕ into a mean value $\overline{\phi}$ and a fluctuation part ϕ' that results from the turbulence flow:

$$\phi = \overline{\phi} + \phi'. \tag{13}$$

Substituting Eq. 13 into the general conservation, Eqs. 1 to 12, and taking the time average over a long period of time yields the momentum, heat, and species balance equations. A set of Reynolds-averaged conservation equations for the mass, heat, momentum, and chemical species for the gaseous, liquid, and solid phases can be written as follows. It should be noted that all of the variables in Eqs. 14 to 25, and those following, represent the mean quantities of vectors, or scalars, in the reactor. The overbars have been omitted for simplicity. For the gas phase:

$$\frac{\partial}{\partial t}(\epsilon_g \rho_g) + \frac{\partial}{\partial x_j}(\epsilon_g \rho_g v_j) = n_k \dot{m}_k \tag{14}$$

$$\frac{\partial}{\partial t}(\epsilon_g \rho_g v_i) + \frac{\partial}{\partial x_j}(\epsilon_g \rho_g v_j v_i) = -\epsilon_g \frac{\partial P}{\partial x_i} + \frac{\partial}{\partial x_j}\left[\mu\left(\frac{\partial v_i}{\partial x_j} + \frac{\partial v_j}{\partial x_i}\right)\right] + \epsilon_g \rho_g g_i + n_k \dot{m}_k v_i + \frac{\rho_p}{\tau_{rp}}(v_{pi} - v_i) + \frac{\rho_k}{\tau_{rk}}(v_{ki} - v_i) - \frac{\partial}{\partial x_j}\left(\epsilon_g \rho_g \overline{v_i' v_j'}\right) \tag{15}$$

$$\frac{\partial}{\partial t}(\epsilon_g \rho_g C_p T) + \frac{\partial}{\partial x_j}(\epsilon_g \rho_g v_j C_p T) = \frac{\partial}{\partial x_j}\left(\lambda \frac{\partial T}{\partial x_j}\right) - \sum_{S=1}^{13} W_S Q_{RS} + n_p Q_p + n_k \dot{m}_k C_{pk} T_k - \frac{\partial}{\partial x_j}\left(\epsilon_g \rho_g \overline{v_j' T'}\right) \tag{16}$$

$$\frac{\partial}{\partial t}(\epsilon_g \rho_g Y_s) + \frac{\partial}{\partial x_j}(\epsilon_g \rho_g v_j Y_s) = \frac{\partial}{\partial x_j}\left(\epsilon_g \rho_g D \frac{\partial Y_s}{\partial x_j}\right) + W_S + n_k \dot{m}_k \alpha_s - \frac{\partial}{\partial x_j}\left(\epsilon_g \rho_g \overline{Y_s' v_j'}\right). \tag{17}$$

For the catalyst particulate phase:

$$\frac{\partial}{\partial t}\rho_p + \frac{\partial}{\partial x_j}(\rho_p v_{pj}) = -\frac{\partial}{\partial x_j}\left(\overline{\rho'_p v'_{pj}}\right) \tag{18}$$

$$\frac{\partial n_p}{\partial t} + \frac{\partial}{\partial x_j}(n_p v_{pj}) = -\frac{\partial}{\partial x_j}\left(\overline{n'_p v'_{pj}}\right) \tag{19}$$

$$\frac{\partial}{\partial t}(\rho_p v_{pi}) + \frac{\partial}{\partial x_j}(\rho_p v_{pj} v_{pi}) = -\epsilon_p \frac{\partial P}{\partial x_i} + \frac{\rho_p}{\tau_{rp}}(v_i - v_{pi})$$

$$-\frac{\partial}{\partial x_j}\left(\rho_p \overline{v'_{pj} v'_{pi}} + v_{pj}\overline{\rho'_p v'_{pi}} + v_{pi}\overline{\rho'_p v'_{pj}}\right) + \frac{\partial}{\partial x_j}\tau_{p,ij} + \rho_p g_i \tag{20}$$

$$\frac{\partial}{\partial t}(\rho_p C_{pp} T_p) + \frac{\partial}{\partial x_j}(\rho_g v_{pj} C_{pp} T_p) =$$

$$-\frac{\partial}{\partial x_j}\left(\rho_p C_{pp}\overline{v'_{pj} T'_p} + v_{pj} C_{pp}\overline{\rho'_p T'_p} + C_{pp} T_p \overline{\rho'_p v'_{pj}}\right)$$

$$-n_p Q_p - n_k Q_k. \tag{21}$$

For the feed-spray droplet phase:

$$\frac{\partial}{\partial t}\rho_k + \frac{\partial}{\partial x_j}(\rho_k v_{kj}) = -\frac{\partial}{\partial x_j}\left(\overline{\rho'_k v'_{kj}}\right) - n_k \dot{m}_k \tag{22}$$

$$\frac{\partial n_k}{\partial t} + \frac{\partial}{\partial x_j}(n_k v_{kj}) = -\frac{\partial}{\partial x_j}\left(\overline{n'_k v'_{kj}}\right) \tag{23}$$

$$\frac{\partial}{\partial t}(\rho_k v_{ki}) + \frac{\partial}{\partial x_j}(\rho_k v_{ki} v_{kj}) =$$

$$\frac{\rho_k}{\tau_{rk}}(v_i - v_{ki}) + \rho_k g_i - n_k \dot{m}_k v_i$$

$$-\frac{\partial}{\partial x_j}\left(\rho_k \overline{v'_{ki} v'_{kj}} + v_{ki}\overline{\rho'_k v'_{kj}} + v_{kj}\overline{\rho'_k v'_{ki}}\right) \tag{24}$$

$$\frac{\partial}{\partial t}(\rho_k C_{pk} T_k) + \frac{\partial}{\partial x_j}(\rho_k v_{kj} C_{pkj} T_k) = n_k m_k C_{pk} \dot{T}_{kl}$$

$$-C_{pk} T_k n_k \dot{m}_k - \frac{\partial}{\partial x_j}\left(\rho_k C_{pk}\overline{v'_{kj} T'_k} + v_{kj} C_{pk}\overline{\rho'_k T'_k} + C_{pk} T_k \overline{\rho'_k v'_{kj}}\right). \tag{25}$$

Turbulence models

The resulting Reynolds averaged equations (Eqs. 15 to 25), contain new unclosed terms related to turbulent flow and reaction, such as: $-\epsilon_g \rho_g \overline{v'_i v'_j}$, $-\rho_P \overline{v'_{pj} v'_{pi}}$, $-\rho_k \overline{v'_{kj} v'_{ki}}$, $-\epsilon_g \rho_g \overline{v'_j Y'_s}$, $-\epsilon_g \rho_g \overline{v'_j T'}$, $-\rho_P \overline{v'_{pj} T'_p}$, and $-\rho_k \overline{v'_{kj} T'_k}$. These terms can be closed by expressing them in terms of mean flow quantities using turbulent models as follows.

In the 3-D, two-phase turbulent flow-reaction model previously mentioned (Gao et al. 1999), the multiphase turbulence model $k-\epsilon$-k_p for both gaseous and catalyst particle phases was established and combined with heat transfer and kinetic reaction models. It accounted for the influences of comparatively high catalyst particle concentration in the FCC riser

Table 1. Auxiliary Expressions for the Catalyst Particle and Feed-Spray Droplet Phases

Items	Catalyst Particle Phase	Feed-Spray Droplet Phase
Relaxation time for particle or droplet flows	$\tau_{rp} = \frac{d_p^2 \bar{\rho}_p}{18\mu}\frac{1}{C_D}\frac{24}{Re_p}$	$\tau_{rk} = \frac{d_k^2 \bar{\rho}_k}{18\mu}\frac{1}{C_D}\frac{24}{Re_k}$
Resistance coeff. of single particle or droplet	$C_{DS} = \begin{cases} 0.44 & Re_p > 1{,}000 \\ \frac{24}{Re_p}(1+0.15\,Re_p^{0.667}) & Re_p \le 1{,}000 \end{cases}$	$C_{DS} = \begin{cases} 0.44 & Re_k > 1{,}000 \\ \frac{24}{Re_k}(1+0.15\,Re_k^{0.667}) & Re_k \le 1{,}000 \end{cases}$
Resistance coeff. of particle or droplet mass	$C_D = C_{DS}\cdot\epsilon_g^{-2.65}$	$C_D = C_{DS}\cdot\epsilon_g^{-2.65}$
Reynolds no. for particle or droplet	$Re_p = d_p \mid \nu - \nu_p \mid /\nu$	$Re_k = d_k \mid \upsilon - \upsilon_k \mid /\nu$
Catalyst particle Nusselt no.	$Nu_p = 0.03 Re_p^{1.3} \quad 0.1 < Re_p < 100$	
Heat transfer between gas and catalyst particle phases	$Q_P = \pi d_p Nu_P \lambda (T_p - T)$	
Heat transfer between spray droplet and catalyst particle phases	$Q_k = \dot{m}_k L + m_k C_{pk} \dot{T}_{kl}$	
Single spray droplet mass		$m_k = \frac{\pi}{6} d_k^3 \bar{\rho}_k$
Varying rate of feed-spray droplet mass		$\dot{m}_k = m_k / t_{\text{vap}}$
Varying rate of feed-spray droplet temp.		$\dot{T}_{kl} = (T_{kb} - T_{k0})/t_k$
Heat transfer between feed-spray and catalyst phases		$n_k m_k C_{pk} \dot{T}_{kl}$
Heat transfer between gas and feed-spray phases		$C_{pk} T_k n_k \dot{m}_k$

reactors on the overall turbulent configuration and described turbulence for catalyst particles using the turbulent kinetic energy k_p transport equation.

A 3-D, three-phase (gas–liquid–solid) flow-reaction model is now being developed. Similarly, the second-order turbulence correlation terms for the third phase, feed-spray droplets in Eqs. 22 to 25 are closed using the Reynolds averaging process and the same gradient hypothesis (Chen and Wood, 1985; Adeniji-Fashola and Chen, 1990) together with the turbulence isotropy hypothesis. For conciseness, the turbulence closure expressions for the feed-spray phase only will be presented below. More details on the closure approach, the eddy-viscosity theory, the turbulence kinetic energy transports, and the reciprocal impacts between both gas and catalyst particle phases can be found in Gao et al. (1999).

$$-\overline{\rho_k' v_{kj}'} = \frac{\nu_k}{\sigma_{kk}} \frac{\partial \rho_k}{\partial x_j} \tag{26}$$

$$-\overline{n_k' v_{kj}'} = \frac{\nu_k}{\sigma_{kk}} \frac{\partial n_k}{\partial x_j} \tag{27}$$

$$-\overline{v_{ki}' v_{kj}'} = \upsilon_k \left(\frac{\partial v_{ki}}{\partial x_j} + \frac{\partial v_{kj}}{\partial x_i} \right) + \frac{2}{3} k_k \delta_{ij} \tag{28}$$

$$-\overline{v_{kj}' T_k'} = \frac{\nu_k}{\sigma_{kk}} \frac{\partial T_k}{\partial x_j} \tag{29}$$

$$\mu_k = \rho_k \nu_k \tag{30}$$

$$\nu_k = C_{\mu k} k_k^{0.5} k^{1.5} / \epsilon, \tag{31}$$

where $k_k = (1/2)\overline{v_{ki}' v_{ki}'}$ is the turbulence kinetic energy of the feed-spray droplet phase. The feed-spray phase turbulence eddy kinematic viscosity, ν_k, is also calculated from Zhou and Huang (1990) and Guo (1995).

The Reynolds stress equation for feed-spray was derived from its momentum equation:

$$\frac{\partial}{\partial t}\left(\rho_k \overline{v_{ki}' v_{kj}'} \right) + \frac{\partial}{\partial x_k}\left(\rho_k \upsilon_{kk} \overline{v_{ki}' v_{kj}'} \right) = D_{k,ij} + P_{k,ij} + \epsilon_{k,ij} \tag{32}$$

where $D_{k,ij}$ and $P_{k,ij}$ are the diffusion and production terms, respectively, and $\epsilon_{k,ij}$ represents the source term resulting from gaseous effects:

$$D_{k,ij} = \frac{\partial}{\partial x_k}\left[C_{ks} \rho_k \frac{k_k}{\epsilon_k} \overline{v_{kk}' v_{kl}'} \frac{\partial}{\partial x_l}\left(\overline{v_{ki}' v_{kj}'} \right) \right] \tag{33}$$

$$P_{k,ij} = -\left(\rho_k \overline{v_{kk}' v_{ki}'} + \upsilon_{kk} \overline{\rho_k' v_{ki}'} \right) \frac{\partial \upsilon_{kj}}{\partial x_k} - \left(\rho_k \overline{v_{kk}' v_{kj}'} + \upsilon_{kk} \overline{\rho_k' v_{kj}'} \right) \times \frac{\partial \upsilon_{ki}}{\partial x_k} + \overline{\rho_k' v_{kj}'} g_i + \overline{\rho_k' v_{ki}'} g_j \tag{34}$$

Table 2. Constants for the Gas–Liquid–Solid Three-Phase Flow-Reaction Model

C_1	1.44
C_2	1.92
σ_k	1.0
σ_ϵ	1.3
σ_p	1.0
σ_{kk}	0.70
C_μ	0.09
$C_{\mu P}$	0.0064
C_p^p	0.80
$C_{\mu k}$	0.0064
C_p^k	0.80

Table 3. Riser Reactor Dimensions and Physical Properties

Reactor dimensions	Unit I	Unit II
Height (m)	32.8	27.35
Height in the disengager (m)	15.4	9.9
Diameter (m)	0.6	0.4
Number of feed nozzles	4	2
Nozzle inclination, θ(°)	30.0	30.0
Physical properties	Unit I	Unit II
Hydrocarbons		
Density (liquid) (20°C) (kg/m^3)	709.4	668.0
Laminar visc. (hydroc. vapor at 550°C) (Pa·s)	2.0×10^{-5}	2.0×10^{-5}
Thermal conduct. (vapor at 550°C) [W/(m·s)]	0.0555	0.0555
Specific heat (liquid) (300°C) [J/(kg·K)]	2,670	2,670
Heat of vaporization (kJ/kg)	155	163
Vaporization temp. (K)	733	698
Avg. molecular wt.	420	373
Strucutral group composition		
Alkylcarbon mass fraction, C_P	0.5588	0.6709
Naphthenic carbon mass fraction, C_N	0.2663	0.0918
Aromatic carbon mass fraction, C_A	0.1749	0.2373
Catalyst		
Particle density (kg/m^3)	1,560	1,500
Specific heat [J/(kg·K)]	1,097	1,097
Particle diameter (μm)	66.0	65.0

Table 4. Operating Parameters

Items	Unit I	Unit II
Feedstock spray		
Mass rate (kg/s)	3.54	2.62
Inject velocity (m/s)	60.0	60.0
Initial temp. (K)	593	563
Inlet vol. fraction	0.0544	0.0547
Avg. diameter (μm)	60	60
Prelift steam		
Mass rate (kg/s)	0.0349	0.0464
Inlet temp. (K)	840.6	875.4
Inlet velocity (m/s)	0.84	1.29
Atomizing steam		
Mass rate (kg/s)	0.088	0.065
Inlet temp. (K)	593	563
Inlet velocity (m/s)	60.0	60.0
Catalysts		
Mass flow rate (kg/s)	17.36	9.93
Inlet temp. (K)	840.6	875.4
Inlet veloc. (m/s)	0.84	1.29
Inlet vol. fraction	0.19	0.08
Outlet pressure (Pa)	2.6×10^5	2.7×10^5

$$\epsilon_{k,ij} = \frac{1}{\tau_{rk}}\Big[\ \rho_k\Big(\overline{v'_{kj}v'_i} + \overline{v'_{ki}\,v'_j} - 2\overline{v'_{ki}v'_{kj}}\Big) + (v_i - v_{ki})\overline{\rho'_k v'_{kj}} + (v_j - v_{kj})\overline{\rho'_k v'_{ki}}\Big]. \quad (35)$$

Then the kinetic energy k_k turbulence equation, shown as Eq. 36, was obtained by making $i = j$ in Eq. 32. Hence, the multiphase turbulence model $k - \epsilon - k_p - k_k$ for gas–liquid–solid three-phase flow-reaction model of the FCC riser reactor is formed by uniting the previous $k - \epsilon - k_p$ model:

$$\frac{\partial}{\partial t}(\rho_k k_k) + \frac{\partial}{\partial x_j}(\rho_k v_{kj} k_k) = \frac{\partial}{\partial x_j}\left(\frac{\mu_k}{\sigma_{kk}}\frac{\partial k_k}{\partial x_j}\right) + \frac{\partial}{\partial x_j}\left(k_k \frac{\nu_k}{\sigma_{kk}}\frac{\partial \rho_k}{\partial x_j}\right) + G_{pk} + G_{gk}, \quad (36)$$

where G_{pk} is the generation rate of k_k, and G_{gk} is a term that changes the feed-spray phase turbulence pattern:

$$G_{pk} = \mu_k\left(\frac{\partial v_{ki}}{\partial x_j} + \frac{\partial v_{kj}}{\partial x_i}\right)\frac{\partial v_{ki}}{\partial x_j} \quad (37)$$

$$G_{gk} = \frac{2\rho_k}{\tau_{rk}}\left(C_p^k\sqrt{kk_k} - k_k\right) + \left(2C_p^k\sqrt{kk_k} - k_k\right)n_k\dot{m}_k + \left(\frac{1}{\tau_{rk}} + \frac{\dot{m}_k}{m_k}\right)\frac{\nu_k}{\sigma_{kk}}(v_i - v_{ki})\frac{\partial \rho_k}{\partial x_i}. \quad (38)$$

It needs to be pointed out that k and ϵ transport equations are different from those in the 3-D, two-phase FCC riser flow-reaction model (Gao et al., 1999). The term G_R is added to embody the impact of feed vaporization on the gaseous phase into the source terms, given by

$$\frac{\partial}{\partial t}(\epsilon_g \rho_g k) + \frac{\partial}{\partial x_j}(\epsilon_g \rho_g v_j k) = \frac{\partial}{\partial x_j}\left(\frac{\mu_e}{\sigma_k}\frac{\partial k}{\partial x_j}\right) + G_k + G_p + G_R - \epsilon_g \rho_g \epsilon \quad (39)$$

$$\frac{\partial}{\partial t}(\epsilon_g \rho_g \epsilon) + \frac{\partial}{\partial x_j}(\epsilon_g \rho_g v_j \epsilon) = \frac{\partial}{\partial x_j}\left(\frac{\mu_e}{\sigma_\epsilon}\frac{\partial \epsilon}{\partial x_j}\right) + \frac{\epsilon}{k}\left[C_1(G_k + G_p + G_R) - C_2\epsilon_g \rho_g \epsilon\right] \quad (40)$$

$$G_R = -k \cdot n_k \cdot \dot{m}_k. \quad (41)$$

Constitutive equations

One of the key constitutive equations models the source term W_s in Eqs. 3, 4, 16, and 17 and requires input from the catalytic cracking kinetic model. The present work also chose the thirteen-lump kinetic model (Sa et al., 1995), proposed for a riser reactor fed with gas oil and vacuum residual blend (see Gao et al. (1999) for details).

Actually, the mass varying rate of a single feed-spray droplet, $\dot{m}_k$, within the basic conservation equations is the vaporization rate of feed-spray. It was reported that the va-

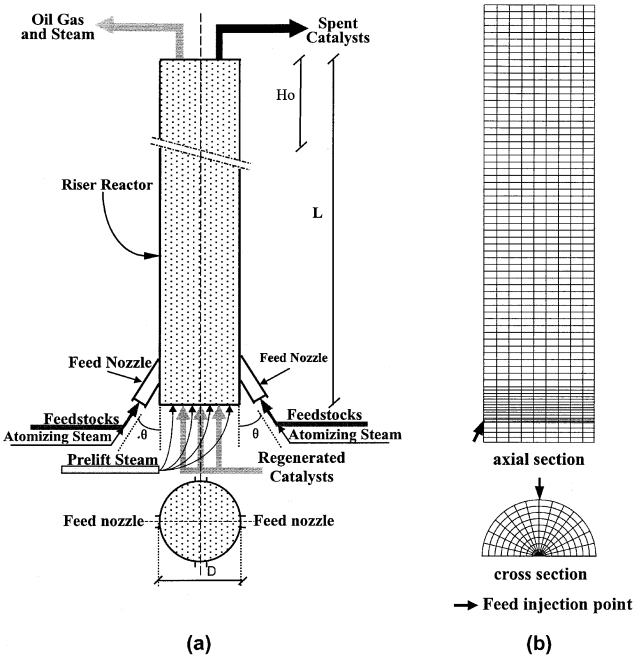

Figure 2. (a) Geometry of FCC riser reactor (containing 4 feed nozzles); (b) computational grid for a riser reactor (Unit II).

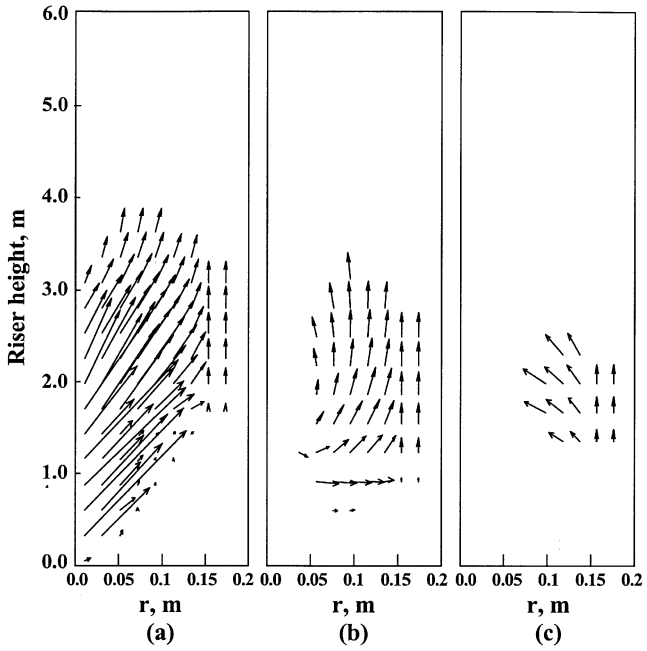

Figure 3. Flow field of the feed spray at various axial sections of Unit II riser reactor.

(a) Across feed nozzle; (b) $\pi/4$ from feed nozzle's axial section; (c) $\pi/2$ from feed nozzle's axial section.

porization of feed containing a portion of vacuum residuum could be completed within 0.2 s if the feed-spray has a droplet size of 60 μm (Liu and Han, 1992). By assuming a constant vaporizing rate and temperature, $\dot{m}_k$ is given by $m_k = \bar{\rho}_k \cdot ((\pi/6)d_k^3)/t_{\text{vap}}$, where $t_{\text{vap}} = 0.2$ s when $d_k = 60\,\mu$m. Meanwhile, the temperature rise rate for feed-spray droplets $\dot{T}_{kl}$ is expressed as $\dot{T}_{kl} = (T_{kb} - T_{k0})/t_k$, where T_{kb} is the temperature at which the feed begins to vaporize, T_{k0} is the initial feed-spray temperature, and t_k is the time of the feed temperature rise, set at 0.2 s.

Other constitutive equations for the catalyst phase and feed-spray phase are listed in Table 1. Table 2 gives the empirically assigned model constants in the gas–liquid–solid 3-phase, flow-reaction model.

The inlet boundary conditions are completely specified for all dependent variables for all the gas feed-spray droplet and catalyst particulate phases to the prescribed flow and reaction conditions. Here, only the boundary conditions for the feed-spray phase are given due to space constraints; those for both the gas and catalyst particle phases can be seen in Gao et al. (1999).

At the feed nozzle inlet of the FCC riser, all variables (with subscript *jet*) for the feed-spray phase are regarded as being uniform; let $u_{k\text{jet}} = v_{\text{jet}} \cdot \cos\theta$, $v_{k\text{jet}} = v_{\text{jet}} \cdot \sin\theta$, $w_{k\text{jet}} = 0$, and set T_{k0}. The $\rho_{k\text{jet}}$ and $n_{k\text{jet}}$ terms are fixed by the imposed feed-spray mass flux Gs (in kg/m^2/s). At the axis of the riser reactor, let $v_k = w_k = 0$ and $\partial\varphi_k/\partial r = 0$. ($\varphi_k = u_k,\ T_k,\ \rho_k,\ n_k,\ k_k$). At the symmetry plane, the normal gradient of these quantities ($u_k,\ v_k,\ T_k,\ \rho_k,\ n_k,\ k_k$) is set to zero and $w_k = 0$, while at the exit, a fully developed flow is described by: $\partial\varphi_k/\partial x = 0$ ($\varphi_k = u_k,\ v_k,\ w_k,\ T_k,\ \rho_k,\ n_k,\ k_k$).

The set of partial differential equations, established for the 3-D, three-phase flow-reaction model for FCC riser reactors, express the conservation of momentum, heat and chemical species. The computational approach to solving these equations uses the SIMPLE (Partankar, 1980) and IPSA (Spalding, 1977) algorithms. Multiple iterations were made on a multi-way coupling to achieve the convergence of the three-phase flow, especially at the feed-injection zone of the riser where feed vaporization as well as cracking reactions are taking place, combining with extensive interrelated connections among the three phases. Specific iteration strategies were mapped out (Gao, 1997). Convergence accuracy for the continuity equations is shown as follows to assure mass conservation:

1. Relative total surplus source of the pressure-correction equation was less than ξ_g for the gas phase

$$\frac{\text{Total surplus source of pressure-correction eq.}}{\text{Inlet total gas mass flux}} < \xi_g. \quad (42)$$

2. Relative total surplus source of continuity equation was less than ξ_P for the catalyst particle phase

$$\frac{\text{Total surplus source of continuity eq.}}{\text{Inlet total catalyst particle mass flux}} < \xi_P. \quad (43)$$

3. Relative total surplus source of continuity equation was less than ξ_P for the feed-spray droplet phase

$$\frac{\text{Total surplus source of continuity eq.}}{\text{Inlet total feed-spray particle mass flux}} < \xi_k, \quad (44)$$

where ξ_g was 0.005–0.01, ξ_P was 0.005–0.01, and ξ_k was 0.01–0.05.

Riser Reactors for Simulations

The riser reactor dimensions and physical properties, as well as the operating parameters for the simulation considered, are presented in Tables 3 and 4, respectively. These data were extracted from 24×10^4 ton/y (Unit I) and 9×10^4

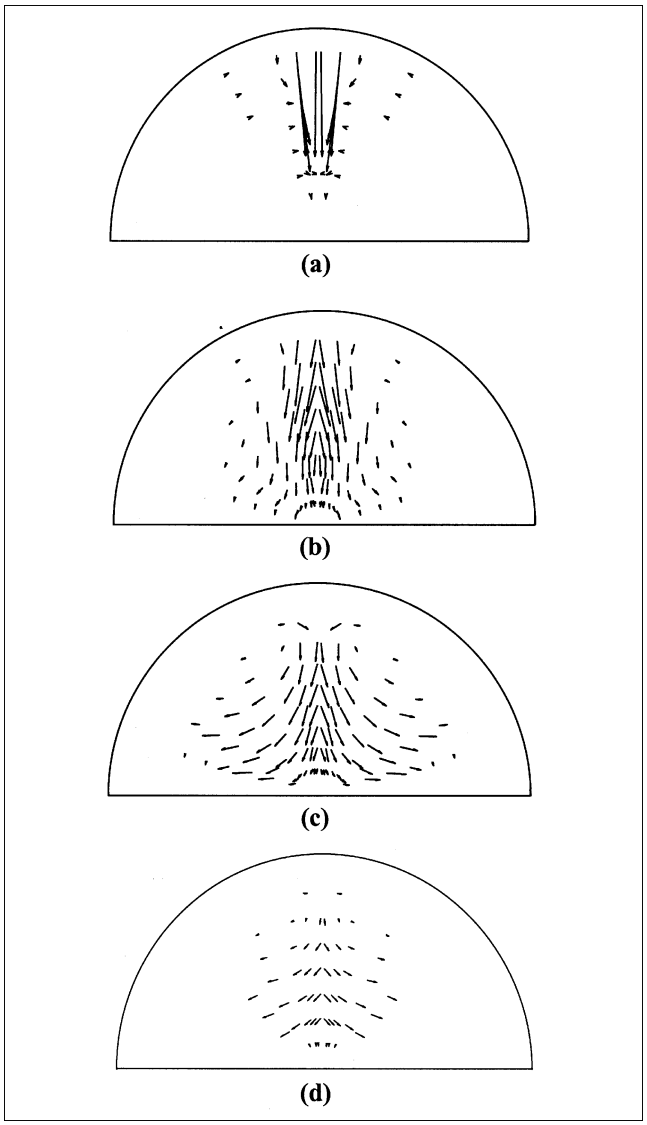

Figure 4. Flow field of the feed spray at various axial distances of the horizontal planes from the feed inlet plane of Unit II riser reactor.
(a) 0.30 m; (b) 0.60 m; (c) 1.5 m; (d) 2.4 m.

ton/y (Unit II) commercial vacuum gas oil FCC units, based on the proposed feed vaporization scheme. Figure 2(a) illustrates the geometry of an FCC riser reactor. For even spacing of feed nozzles around the circumference of the feed-injection zone, the spray symmetry pattern repeats itself in every sector containing one feed nozzle. Consequently, the computational integration domain was restricted in the circumferential direction to only one sector containing one feed nozzle. The operating parameters and boundary conditions given in Table 3 are based on one feed nozzle sector. The computational grid used consists of $75 \times 10 \times 15 = 11{,}250$ mesh cells in the axial, radial, and tangential coordinates, see Figure 2 (b).

Results and Discussion

The present study has developed a separate set of governing equations for the feed-spray, regarded as a separate phase, including the continuity equation, the momentum equation, the enthalpy equation, and the turbulent kinetic energy equation. Moreover, the extensive coupling among the feed-spray, the gaseous phase, and the catalyst was incorporated into the integrated three-phase flow-reaction model. Full 3-D, three-phase simulations performed on commercial FCC riser reactors provided details on the flow field, the temperature, and the concentration fields for gaseous and solid phases, as well as a distinct image of feed-spray flow and vaporization.

Flow of feed-spray

Figure 3 shows the flow fields of the feed-spray phase at various vertical planes across the circumferential axis from the feed inlet plane (the axial sections) of Unit II (Table 3). Figure 4 is the flow fields for the feed-spray phase, at various axial distances, of the horizontal planes from the feed inlet plane. Figures 3 and 4 show that the feed-spray injection into the reactor causes flow inhomogeneities in all directions in the vicinity of the feed nozzles, where recycling flows persist. The feed injecting zone at the riser base shows the most complex patterns. An obvious flow pattern is also seen in Figure 3, where, because of occluded gaseous phase, the feed-spray phase is directed toward the riser axis from the wall at the axial section across from the feed nozzle. The direction changes to nearly parallel to the axis at the vertical plane, $\pi/4$ away from the feed inlet plane and toward the side wall from the axis, $\pi/2$ away from the inlet plane. This corresponds to the recycling flow pattern in Figure 4. The flow of the feed-spray phase works in a similar way to the gaseous phase. From Figures 3 and 4, it can be determined that complete feed vaporization takes places over the first 4 m of the riser reactor.

The feed-spray zone

Data for the feed-spray area, representing the processes of feed-spray flow and vaporization inside the FCC riser reactors, when processed through the proposed three-phase flow-reaction model, allows an entire 3-D picture of the feed-spray area to be imaged. The model was also used to determine the impact of these processes on the cracking reactions. Figures 5 and 6 show the contour diagrams for the feed-spray droplet concentrations at various vertical axial sections and at various horizontal planes, respectively.

Because of the oblique injection upward of feed-spray and atomizing steam from the riser side at an angle of 30° from

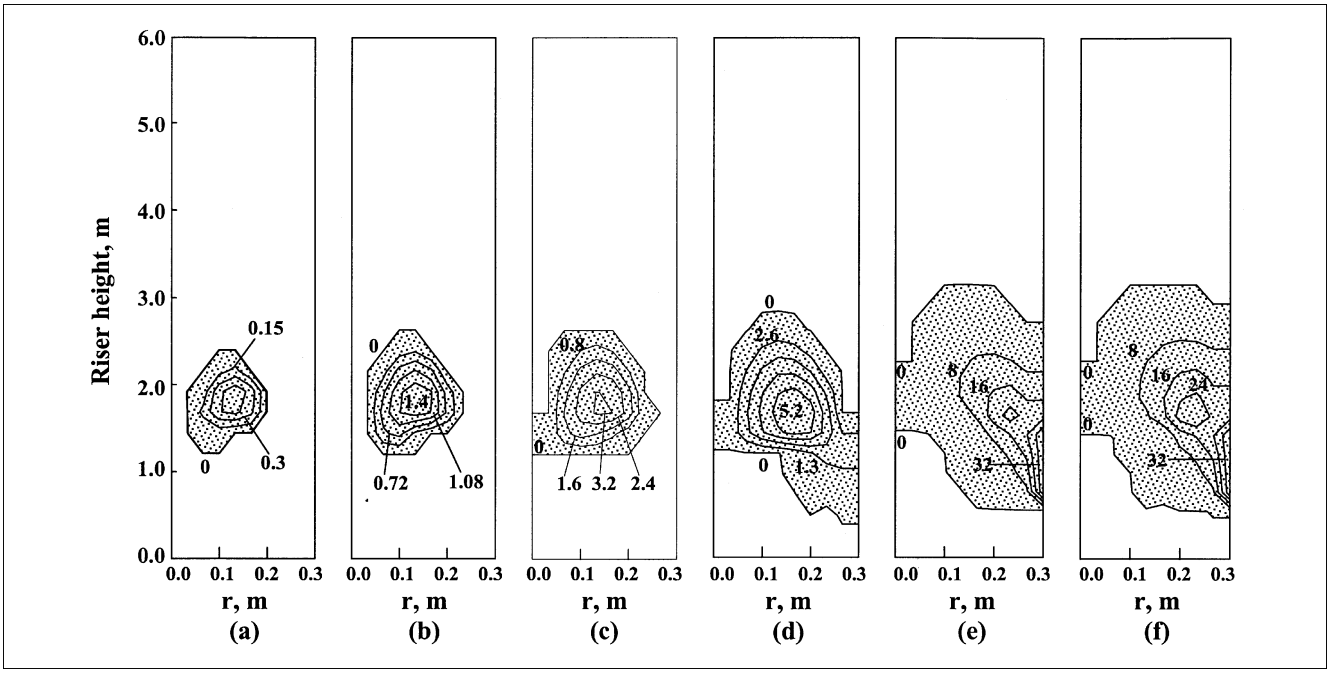

Figure 5. Feed-spray area at various axial sections of Unit I riser reactor (feed-spray droplet concentrations, kg/m^3).

(a) 33.0° from feed nozzle's axial section; (b) 22.5° from feed nozzle's axial section; (c) 15.0° from feed nozzle's axial section; (d) 7.6° from feed nozzle's axial section; (e) 3.8° from feed nozzle's axial section; (f) across feed nozzle.

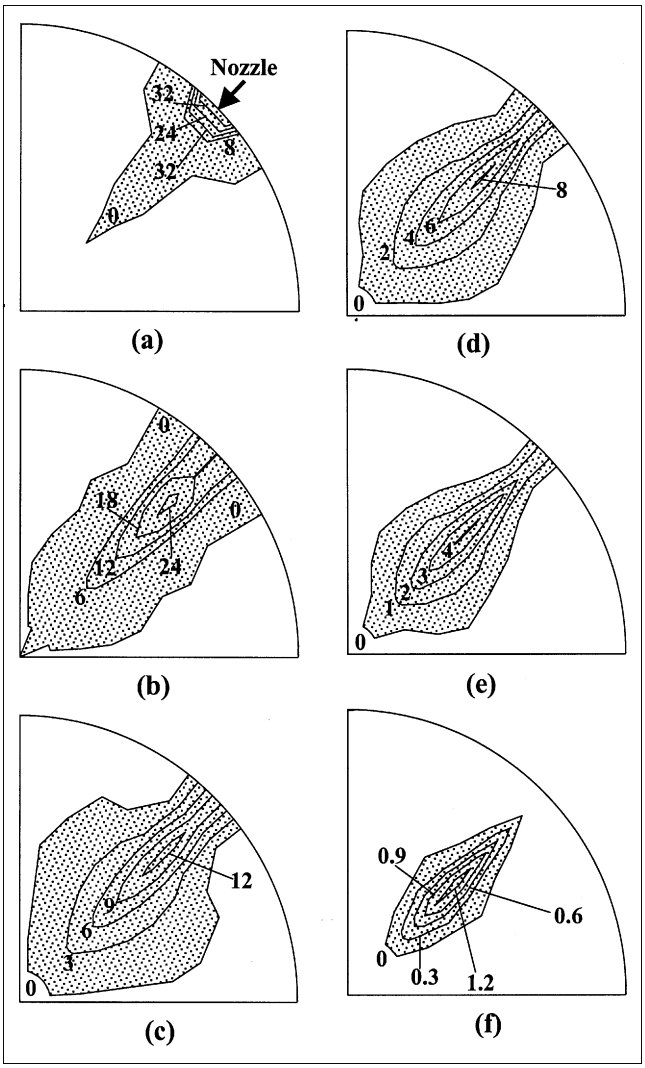

Figure 6. Feed-spray area at various cross sections of Unit I riser reactor (feed-spray droplet concentrations, kg/m^3).

(a) across feed nozzle; (b) 0.40 m; (c) 1.2 m; (d) 2.0 m; (e) 2.8 m; (f) 3.6 m.

the riser axis, the feed-spray area was smaller in the lower riser cross sections. It becomes bigger with riser height, but at a certain point it grows gradually smaller as the feed-spray phase vaporization continues. Observed at various vertical planes across the circumferential axis, the feed-spray occupies the biggest area at the feed inlet plane, becoming gradually smaller as the vertical section is moved away. Sequentially, corresponding changes in the diameter, the concentration, and the temperature of the feed-spray droplets occurred everywhere within the feed-spray area. Figures 7 and 8 show the contour diagrams for the feed-spray droplet diameters at various axial sections and cross sections, respectively. Figures 9 and 10 show the contour diagrams for the feed-spray temperatures at various axial sections and cross-sections, respectively.

It is obvious from Figures 5 to 8 that the concentration and diameter of feed-spray droplets also decrease as the feed-

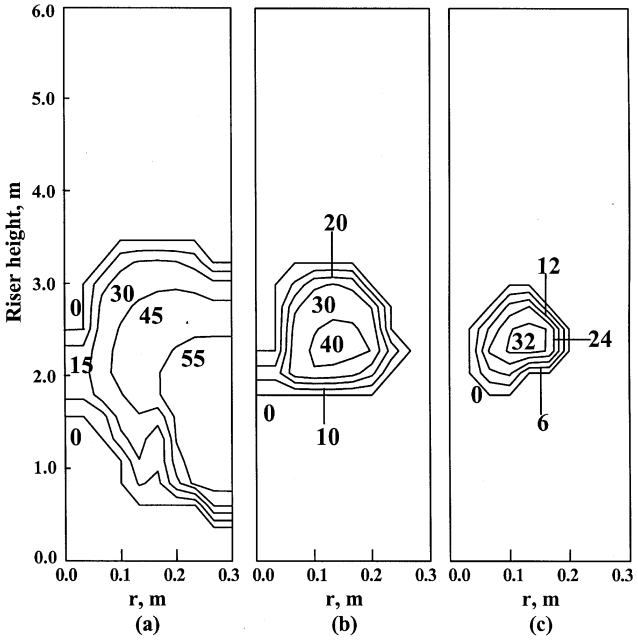

Figure 7. Feed-spray droplet diameter (μm) distribution at various axial sections of Unit I riser reactor.

(a) Across feed nozzle; (b) $\pi/8$ from feed nozzle's axial section; (c) $\pi/4$ from feed nozzle's axial section.

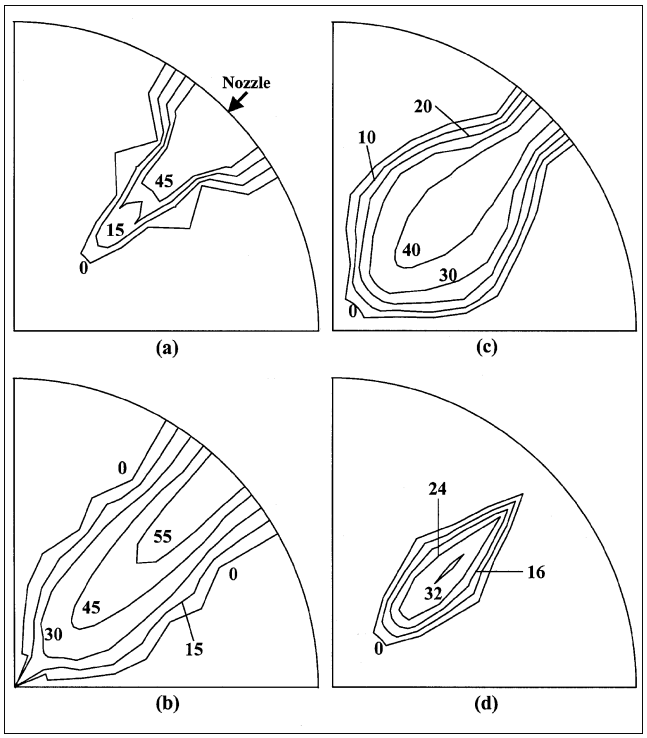

Figure 8. Feed-spray droplet diameter (μm) distribution at various cross sections of Unit I riser reactor.

(a) Across feed nozzle; (b) 0.40 m; (c) 2.0 m; (d) 3.6 m.

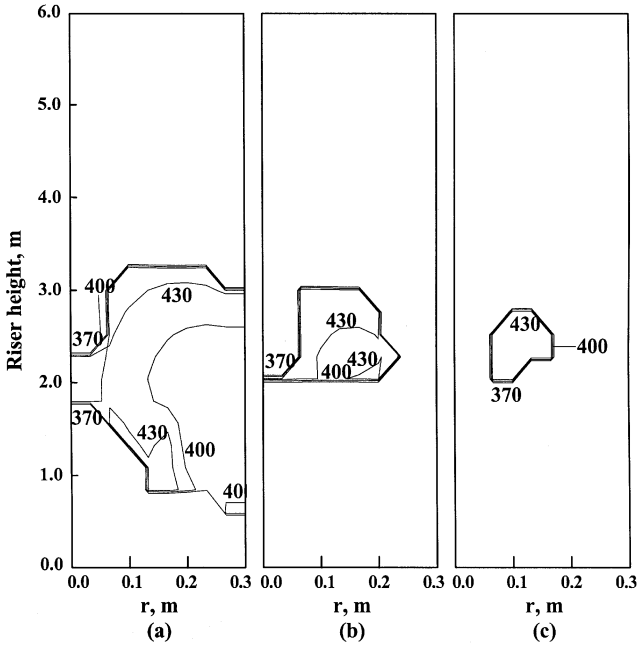

Figure 9. Feed-spray temperature (°C) distribution at various axial sections of Unit I riser reactor.

(a) Across feed nozzle; (b) $\pi/8$ from feed nozzle's axial section; (c) $\pi/4$ from the feed nozzle's axial section.

spray flow and vaporization progress. Figures 9 and 10 reflect the corresponding temperature rise of feed-spray droplets during the flow and vaporization. Complete vaporization took place when the feed-spray temperature reached the vaporizing temperature 460°C. This occurs at the edge of the feed-spray zone. In summary, all of these observations characterize the feed-spray during its stay inside the riser reactor. It is the complex feed vaporization that exerts significant influence on the flow, heat transfer, and cracking reactions occurring inside FCC riser reactors.

Heat transfer and reaction

With regard to the resulting flow and reaction throughout the riser reactor, intensive nonuniform distribution of all dependent variables was still predicted, especially at the bottom of the riser. This is in accordance with the result of the earlier two-phase turbulent flow-reaction model (Gao et al.,

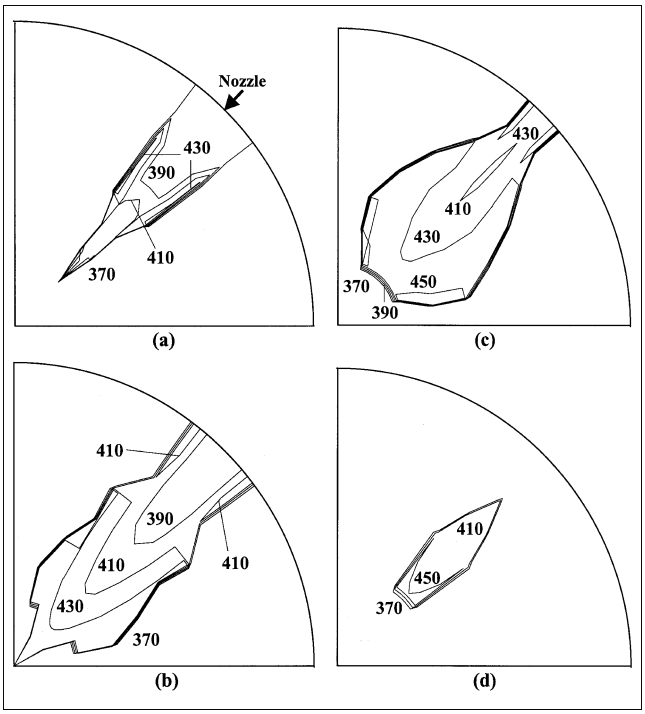

Figure 10. Feed-spray temperature (°C) distribution at various cross-sections of Unit I riser reactor.

(a) Across feed nozzle; (b) 0.40 m; (c) 2.0 m; (d) 3.6 m.

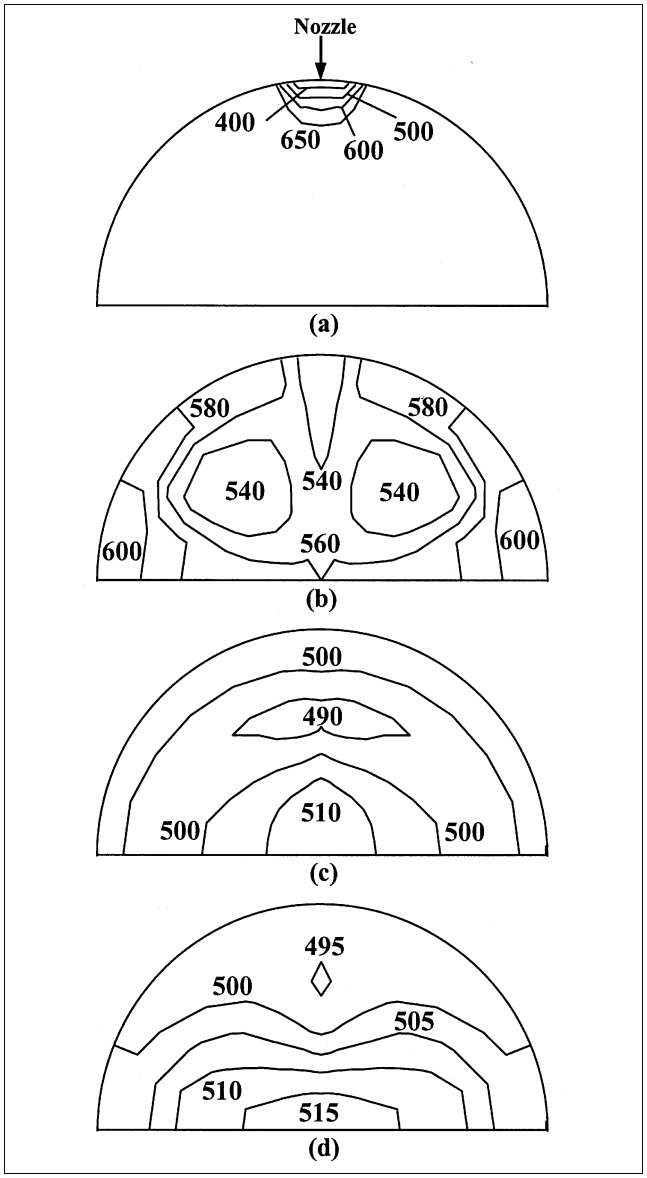

Figure 11. Contour of gas temperature (°C) at various cross sections of the riser reactor (Unit II).

(a) Across feed nozzle; (b) 1.2 m; (c). 5.4 m; (d) 10.2 m.

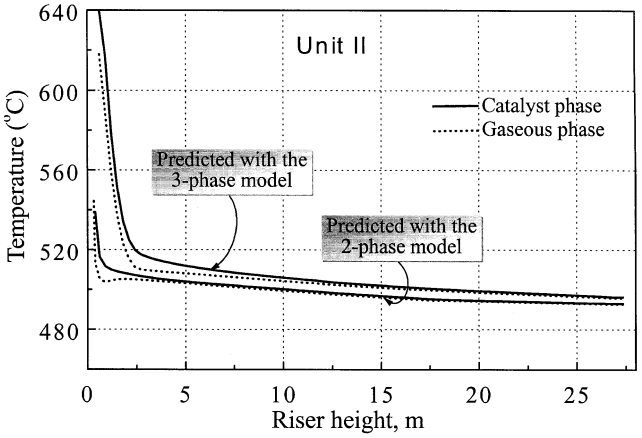

Figure 12. Temperature distribution of gas and solid phases along the riser height (Unit II).

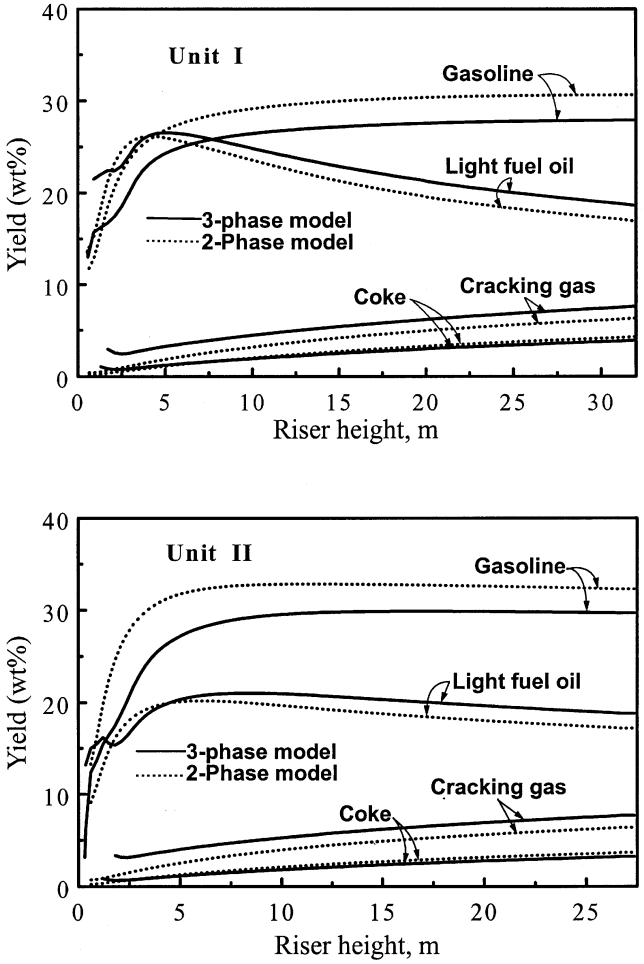

Figure 13. Composition distribution of gas phase along the riser reactor height.

1999). However, there were some obvious changes in the heat-transfer and cracking reactions after including the vaporization of feed-spray in the gas–liquid–solid three-phase flow-reaction model. In particular, the representative temperature distribution in the gaseous phase showed intensive inhomogeneities, with a gradient of tens of degrees, within the feed-spray zone (see Figure 11). The main reason for this is that much more heat transfer is needed to raise the feed to vaporization temperature, and this reality is taken into account in the three-phase flow-reaction model.

Figure 12 shows the predicted mean temperatures of both gaseous and catalyst particle phases along the height of the Unit II riser; those obtained from the earlier two-phase turbulent flow-reaction model are also included. A sharper temperature decrease in the feed inlet zone for the two-phase model is noted owing to the heat requirement needed to increase the feed temperature from its boiling point to the two-phase mixture temperature, assuming instant vaporization of feed. A more gentle decrease in the same zone for the three-phase flow-reaction model is accounted for by better modeling of the actual feed vaporization process occurring inside the riser reactor. It may be deduced that the three-phase flow-reaction model is more reasonable and more reliable than the two-phase one.

Figure 13 shows the distribution of the gaseous component yields, averaged over the cross section along the riser height, for the two reactor units; again, those obtained from the two-phase model are also included. Table 5 compares the predicted temperatures and yields at the riser exit with those from the commercial operation and the two-phase model. These results show a tendency for the resulting cracking reactions to be involved in the three-phase flow-reaction model after feed vaporization. A comparison between the predictions from the three-phase and two-phase models shows similar component distribution profiles but different actual compositions. Thus, the reasonability and reliability of the two-phase model have been passed to the three-phase model. Also, it is shown that cracking reactions are significantly influenced by different feed vaporization modeling methods.

Table 5. Predicted vs. Actual Temperatures and Yields at the Riser Reactor Exits

Unit	Items	T_{out} (°C)	Heavy Fuel Oil (wt. %)	Light Fuel Oil (wt. %)	Gasoline (wt. %)	Cracking Gas (wt. %)	Coke (wt. %)
I	Pred. with three-phase model	505	41.9	18.5	27.8	7.6	3.9
	Pred. with two-phase model	503	41.9	16.9	30.6	6.3	4.3
	Actual	504	42.0	18.5	27.9	7.7	3.9
II	Pred. with three-phase model	496	40.6	18.8	29.7	7.7	3.2
	Pred. with two-phase model	493	40.5	17.2	32.3	6.4	3.6
	Actual	496	40.4	18.8	29.7	7.8	3.3

The critical status of the feed-injection zone and the importance of modeling feed vaporization correctly are established. The results predicted by the three-phase model show a better agreement with measured values from commercial operation than those from the two-phase case. This suggests that the three-phase model can also be used for performance simulation in commercial riser reactors.

Operation Modification Study

Good atomization of the feed is of importance for fast feed-spray vaporization and improved product distribution. Faster feed-spray vaporization and better mixing with catalysts will result in more uniform cooling of catalyst particles and a consequent reduction in undesired thermal cracking. The feed-spray droplet diameters determine the time for complete vaporization and further influence the flow, heat transfer and cracking reactions occurring in the feed-injection zone. Consequently, the effect of feed-sprays with various droplet diameters on overall riser performance is evaluated in the present work.

The simulation study is based on the Unit II riser reactor and carried out for three initial feed-spray diameters (40 μm, 60 μm and 80 μm) at the same operation conditions, shown in Tables 3 and 4. In view of the complete vaporization of feed-spray with a 60-μm initial diameter within 0.2 s (Liu and Han, 1992), the vaporization times for feed-sprays with 40-μm and 80-μm initial diameters were deduced to be 0.09 s and 0.36 s, respectively, based on the d^2 rule (Zhou, 1986):

$$d_{k1}^2/d_{k2}^2 = t_{k1}/t_{k2}, \tag{45}$$

where d_{k1} and d_{k2} are two different feed-spray initial diameters, and t_{k1} and t_{k2} are their corresponding vaporization times.

In essence the variation of feed-spray droplet diameter causes a change in both vaporization rate and feed-spray volume inside the riser reactor. Figures 14 and 15 present the feed-spray areas for various initial droplet diameters at the vertical axial plane across the feed nozzle and at the axial plane $\pi/3$ apart from the feed nozzle axial plane, respectively. It is shown that the feed-spray zone shrinks with decreasing initial spray diameter at the same cross sections, reflecting the promotion of vaporization for smaller droplets. The values on Figures 14 and 15 give the contour distribution for the spray droplet concentrations; lower spray droplet concentrations are shown at the spray area borders. Figures 16 and 17 show the distributions of feed-spray diameters for various initial diameters during vaporization at the same planes as in Figures 14 and 15, respectively. This is also illustrated in the progress of feed-spray vaporization showing no spray droplets at the edges of the spray areas. The smaller the initial spray diameter, the smaller the spray area.

The effects of various initial feed-spray diameters on the overall reactor performance are shown in Figure 18. These plots depict the variation of light fuel oil, gasoline, cracking gas, and coke yields along the riser height. Distinct changes in all product yields can be seen. These changes result mainly from the variation of feed-spray vaporization time and temperature distribution. Table 6 compares the overall yields for

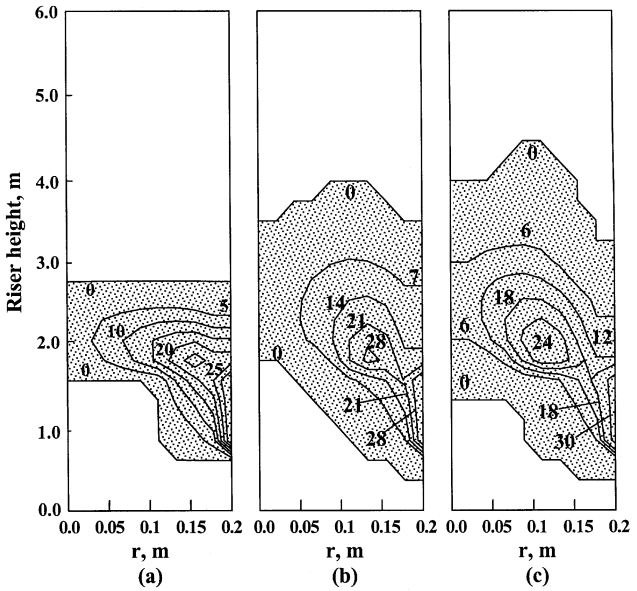

Figure 14. Areas of feed sprays with various initial droplet diameters at the axial section across feed nozzle (feed-spray droplet concentrations, kg/m^3).

(a) Initial spray diameter 40 μm; (b) initial spray diameter 60μm; (c) initial spray diameter 80 μm.

various initial spray droplet diameters. It was shown on Figure 18 and in Table 6 that the overall product distributions improved with a decrease in feed-spray droplet diameter. The gasoline yield increases from 29.5 wt.% to 30.7 wt. % while

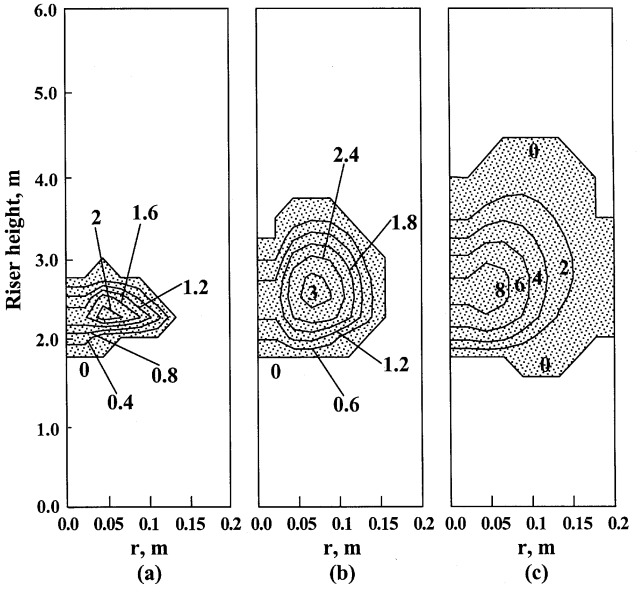

Figure 15. Areas of feed sprays with various initial droplet diameters at the axial section $\pi/3$ from feed nozzle's axial section (feed-spray droplet concentrations, kg/m^3).

(a) Initial spray diameter 40 μm; (b) initial spray 60 μm; (c) initial spray diameter 80 μm.

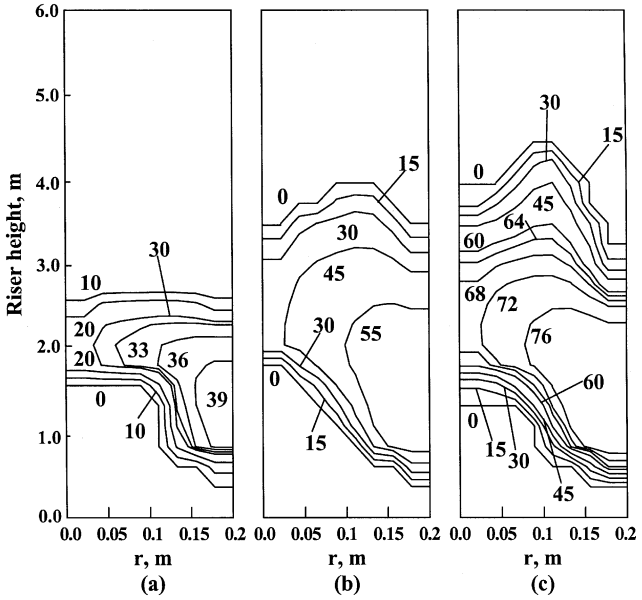

Figure 16. Feed-spray droplet diameter (μm) distribution at the axial section across the feed nozzle.

(a) Initial spray diameter 40 μm; (b) initial spray diameter 60 μm; (c) initial spray diameter 80 μm.

the cracking gas and coke yields have definite decreases from 7.6 wt.% to 7.0 wt.% and from 3.3 wt % to 3.2 wt.%, respectively. However, the light fuel oil yield decreases only from 18.9 wt.% to 18.4 wt.%. This demonstrates that better atomization of feed can result in a more desirable product distribution.

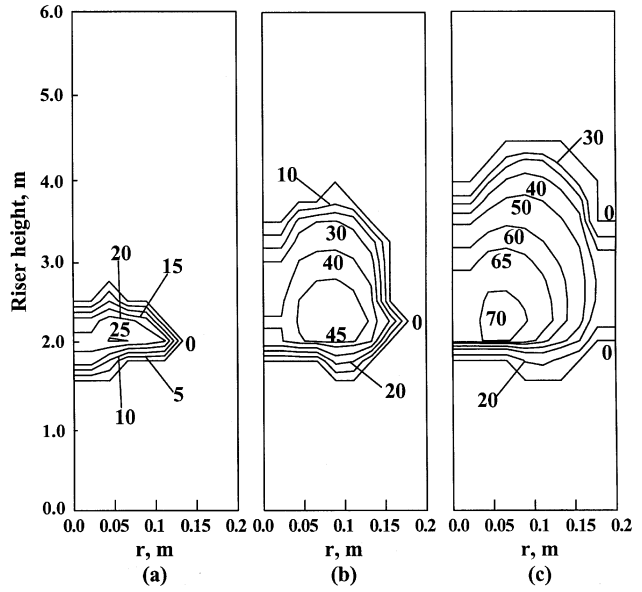

Figure 17. Feed-spray droplet diameter (μm) distribution at the axial section $\pi/3$ from the feed nozzle's axial section.

(a)Initial spray diameter 40 μm; (b) initial spray diameter 60 μm; (c) initial spray diameter 80 μm.

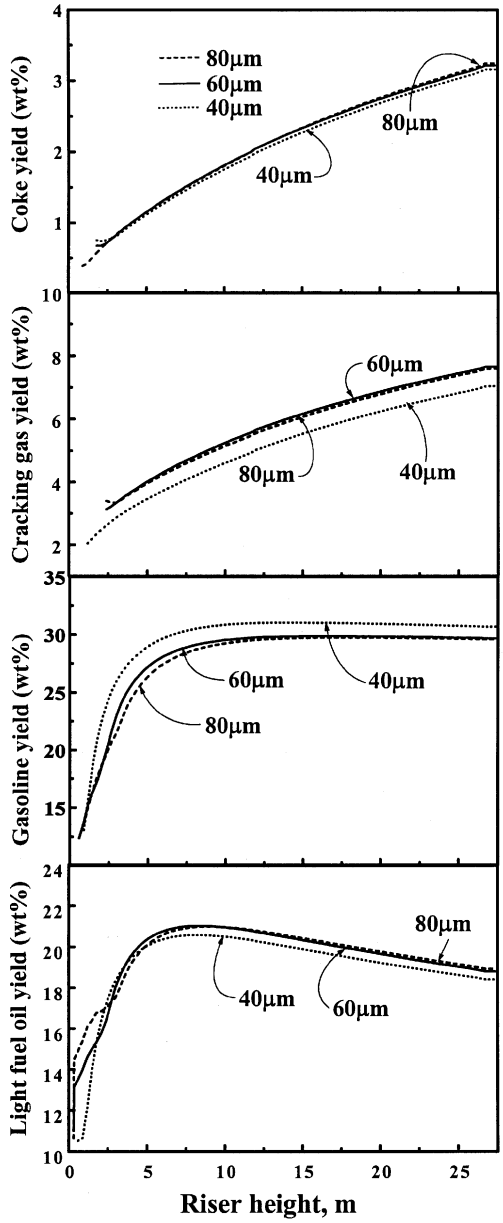

Figure 18. Variation of mean light fuel oil, gasoline, cracking gas and coke yields along the riser height with various feed spray initial diameters.

Table 7 presents the results predicted by the two-phase flow-reaction model (Gao et al., 1999) and by the three-phase flow-reaction model for the same commercial FCC units. It is

Table 6. Predicted Temperature and Yields at the Riser Reactor Exit

			Product Yields (wt. %)			
d_k (μm)	T_{out} (°C)	Heavy Fuel Oil (wt. %)	Light Fuel Oil	Gasoline	Cracking Gas	Coke
40	494.0	40.6	18.4	30.7	7.0	3.2
60	496.0	40.7	18.8	29.7	7.7	3.2
80	496.4	40.6	18.9	29.5	7.6	3.3

Table 7. Two-Phase Flow-Reaction Model vs. the Three-Phase Flow-Reaction Model

Unit	Model	T_{out} (°C)	Heavy Fuel Oil (wt. %)	Light Fuel Oil (wt. %)	Gasoline (wt. %)	Cracking Gas (wt. %)	Coke (wt. %)
I	Two-phase	503	41.9	16.9	30.6	6.3	4.3
	Three-phase	505	41.9	18.5	27.8	7.6	3.9
II	Two-phase	493	40.5	17.2	32.3	6.4	3.6
	Three-phase	496	40.6	18.8	29.7	7.7	3.2

Source: Data on two-phase model from Gao et al. (1999).

noteworthy that the results in Table 7 also imply the effects of various initial feed-spray diameters on the overall cracking reactions. This is because the two-phase model essentially assumes an extreme feed-injection condition, that is, instantaneous feed vaporization, with the necessary heat for vaporization being supplied by regenerated catalyst once the feed-spray enters the riser. Feed injected in this way is equivalent to a feed-spray with 0 μm diameter being fully vaporized within zero time and converted into a uniform gaseous phase. Under these conditions uneven gas-phase temperature distribution and uneven cooling of catalyst particles cannot occur. The gasoline yield increases 2.8 wt. % and 2.6 wt.% and the cracking gas yield decreases 1.2 wt.% and 1.3 wt.% for the two commercial FCC units, respectively. However, the light fuel oil yield declines by 1.6 wt. % and the coke yield increases 0.4 wt.%; this might be explained by the requirement that the overall hydrogen balance must be maintained during the FCC process. The decrement of light fuel oil yield and the increment of coke yield makes hydrogen available for the production of more gasoline. If gasoline is desired, it is beneficial for the feed-spray vaporization to take place according to the assumption in the two-phase flow-reaction model.

In summary, the feed-spray droplet sizes not only affect the feed vaporization but also the overall performance of the riser reactors. According to the scope of the present work, smaller feed-spray diameters provide more desirable product yields. The simulation results from the two-phase flow-reaction model also reflect the overall flow and reaction inside FCC riser reactors under an extreme feed-injection condition.

Conclusions

In order to account for feed vaporization, a 3-D, gas–liquid–solid three-phase flow-reaction model has been developed by establishing another, separate set of governing equations for the feed-spray droplets. This three-phase flow-reaction model is based on a 3-D, two-phase turbulent flow-reaction model (Gao et al. 1999), incorporating thirteen-lump kinetics for residuum cracking reactions (Sa et al. 1995). It can be applied to reveal details on the motion, the temperature rise, and vaporization of feed-spray droplets as well as their impacts on the cracking reactions. In addition, other engineering aspects of the reacting flow in an FCC riser reactor may be elucidated. The predicted results show that complete feed vaporization takes place in the riser reactor within the first 4 m from the spray injection zone after spray injection. Corresponding changes in the diameter, the concentration and the temperature of the feed-spray occurred everywhere within the feed-spray volume. Model predictions are compared with commercial riser reactor operating data and results from the two-phase model. Some obvious changes in heat transfer and cracking reactions occurred when feed-spray vaporization is modeled. These represent the impacts of the feed-spray vaporization on the overall cracking reactions.

An operation modification study to evaluate the effect of feed-spray droplet size was carried out. It is shown that the selectivity to primary products is improved by reducing the initial feed-spray diameter from 80 μm to 40 μm. The decrement of the feed-spray diameters changes the feed vaporization progress and subsequently affects the resulting heat transfer, and cracking reactions. The three-phase flow-reaction model described here can serve as an improved design tool for FCC riser operation case studies because it adequately addresses feed vaporization. The model predictions present the main hydrodynamics, heat transfer and cracking reaction aspects of the FCC process, as well as the feed-spray vaporization progress.

Acknowledgments

We gratefully acknowledge the financial support from the CNPC (China Natural Gas and Petroleum Corporation) and the SINOPEC (China PetroChemical Corporation) for this study.

Notation

C_1, C_2 = turbulent model constants
C_D, C_{DS} = drag force coefficients between fluid and particle
C_{ks} = coefficient of Reynolds stress equation diffusion term
C_p = specific heat of gas phase, J/kg/K
C_{pk} = specific heat of feed-spray droplet, J/kg/K
C_p^k = interaction coefficient between gas and feed-spray droplet phases
C_p^P = interaction coefficient between gas and catalyst particle phases
$C_{\mu k}, C_{\mu p}$ = turbulent model constants
C_{pp} = specific heat of catalyst particle, J/kg/K
D = diffusion coefficient, m^2/s, diameter of riser reactor, m
d_k = initial diameter of feed-spray droplet, m
d_p = diameter of catalyst particle, m
G_k = generation rate of gas turbulent kinetic energy, $kg/m/s^3$
G_p = interaction term between gas and catalyst phases, $kg/m/s^3$
g_i = gravity component in the i coordinate direction, m/s^2
H_0 = length of the disengager, m
k = turbulent kinetic energy of the gas phase, m^2/s^2
L = length of riser reactor, m; latent heat of feed-spray vaporization, J/kg
m_k = mass varying rate of a single feed-spray droplet, kg/s
n_k = number density of feed-spray droplet, $1/m^3$
n_p = number density of catalyst particle phase, $1/m^3$
N = number of feed nozzles
Nu = Nusselt number
P = pressure, Pa
Q_k = the heat transferred from catalyst phase to feed-spray phase, $J/m^3/s$
Q_p = convection heat transfer flux, $J/m^3/s$

Q_{RS} = endothermic capacity of the reactions of the s component, J/kg
r = radial distance, m
Re = Reynolds number
T = temperature, K
t = time, s
t_{vap} = time for complete vaporization of feed-spray, s
u = axial velocity, m/s
v = radial velocity, m/s
v_i, v_j = velocity components of gaseous phase in different coordinates, m/s
v_{pi}, v_{pj} = velocity components of catalyst particle phase in different coordinates, m/s
v_{ki}, v_{kj} = velocity components of feed-spray phase in different coordinates, m/s
v_{jet} = feed-spray efflux velocity, m/s
w = tangential velocity, m/s
W_S = cracking reaction rates, kg/m3/s
x = axial distance of risers, m
x_i, x_j = spatial coordinate, m
Y_s = mass fraction of s component in the gas phase

Greek letters

δ_{ij} = unit tensor
ϵ = dissipation rate of turbulent kinetics energy of the gaseous phase, m^2/s^2
ϵ = volume fraction
λ = coefficient of heat conductivity, W/m/K
μ = dynamic viscosity, kg/m/s
μ_e = effective dynamic viscosity, kg/m/s
ν = kinematic viscosity, m^2s
θ = angle of the axis and nozzle, degree
ρ_g = density of gaseous phase, kg/m^3
ρ_p = apparent density of catalyst particle, kg/m^3
ρ_k = apparent density of feed-spray droplet, kg/m^3
$\bar{\rho}_P$ = catalyst particle density, kg/m^3
$\bar{\rho}_k$ = feed-spray droplet density, kg/m^3
$\sigma_k, \sigma_{kk}, \sigma_\epsilon$ = empirical numbers similar to turbulent Prandtl-Schmidt numbers
$\tau_{p,ij}$ = viscous strain tensor of catalyst particle phase, $kg/m/s^2$
τ_{rk} = the time scale characterizing the response for a single spray droplet, s
τ_{rp} = the time scale characterizing the catalyst particle response, s
ξ = convergence accuracy

Subscripts

g = gas phase
i, j = symbol for spatial coordinates
k = feed-spray phase
p = catalyst solid phase
S = gaseous component

Specific symbols

— = Reynolds time-average value
′ = fluctuation value

Literature Cited

Adeniji-Fashola, A., and C. P. Wood, "Modeling of Confined Turbulent Fluid-Partical Flows Using Eulerian and Lagrangian Schemes," *Int J. Heat Mass Transfer*, **33**, 691 (1990).

Chen, C. P., and P. E. Wood, "A Turbulent Closure Model for Dilute Gas-Particle Flows," *Can. J. of Chem. Eng.*, **63**, 349 (1985).

Chen, J. W., "The Development of the Application of Fluidization Technology in China's Petroleum Refining Industry During the Past 20 Years," *Acta Pet. Sin. (Pet. Process. Sect.)*, **1**, 1 (1985).

Chen, J. W., and H. C. Cao, *Technology and Engineering of Fluidized Catalytic Cracking*, China Petrochemical Press, Beijing, pp. 788, 864 (1995).

Dean, R., J. L. Mauleon, and W. Letzsch, "Total Introduces New FCC Process," *Oil Gas J.*, **80**, 168 (1982)

Gao, J. S., "Numerical Simulation on the Flow, Heat Transfer and Reaction in the Catalytic Cracking Riser Reactors," PhD Diss., Univ. of Petroleum, Beijing, China (1997).

Gao, J. S., C. M. Xu, S. X. Lin, G. H. Yang, and Y. C. Guo, "Advanced Model for Turbulent Gas-Solid Flow and Reaction in FCC Riser Reactors," *AIChE J.*, **45**, 1095 (1999).

Guo, Y. C., "A Pure Two-Fluid Model of Reacting Two-Phase Flows and Its Application in Pulverized Coal Combustion," PhD Diss., Tsinghua Univ., Beijing, China (1995).

Liu, D. L., and J. M. Han, "Evaluation on Commercial Application of LPC Type Nozzle for FCC Feed," *Pet. Process. Eng.*, **22**, 49 (1992).

Mauleon, J. L., and J. C. Courelle, "FCC Heat Balance Critical for Heavy Fuels," *Oil Gas J.*, **83**, 64 (1985).

Mo, W. J., S. X. Lin, G. X. Wang, and G. H. Yang, "Dynamics of Resid Catalytic Cracking Process in the Pilot Plant with a Downflow Transfer Reactor: I. The Pilot Plant and Its Experimental Results," *Acta Pet. Sin. (Pet. Process. Sect.)*, **7**, 1 (1991a).

Mo, W. J., S. X. Lin, G. X. Wang, and G. H. Yang, "Dynamics of Resid Catalytic Cracking Process in the Pilot Plant with a Downflow Transfer Reactor: II. Analysis and Discussion of Plant Results," *Acta Pet. Sin. (Pet. Process. Sect.)*, **7**, 8 (1991b).

Murphy, J. R., "Evolutionary Design Changes Mark FCC Process," *Oil Gas J.*, **90** (20), 49 (1992).

Patankar, S. V., *Numerical Heat Transfer and Fluid Flow*, Hemisphere, Washington, DC, p.146 (1980).

Sa, Y., X. Liang, X. Chen, and J. Liu, "Study on the 13-Lump Kinetic Model for Residual Catalytic Cracking," *Selective Papers in Memorial of 30th Anniversary of the Fluid Catalytic Cracking Process in China*, Luoyan Petrochemical Eng. Corp., Luoyang, China, p.145 (1995).

Schuurmans, H. J. A., "Measurements in a Commercial Catalytic Cracking Unit," *Ind. Eng. Chem. Process Des. Dev.*, **19**, 267 (1980).

Spalding, D. B., *Turbulent Buoyant Convection*, N. Afgan and D. B. Spalding, eds., Hemisphere, Washington, DC, p. 569 (1977).

Theologos, K. N., and N. C. Markatos, "Advanced Modeling of Fluid Catalytic Cracking Riser-Type Reactors," *AIChE J.*, **39**, 1007 (1993).

Theologos, K. N., I. D. Nikou, A. I. Lygeros, and N. C. Markatos, "Simulation and Design of Fluid Catalytic Cracking Riser-Type Reactors," *AIChE J.*, **43**, 486 (1997).

Xie, R. H., "The New Favorite of Petroleum Refining Circle: Heavy Oil Catalytic Cracking," *Petroleum*, **21**, 34 (1985).

Xu, C. M., L. G. Lu, S. X. Lin, and Q. L. Tang, "Catalytic Cracking Reaction Pathway and On-Line Sampling in Commercial Riser," *J. Univ. of Pet.*, China, **21**, 4 (1997).

Zhou, L. X., *Combustion Theory and Chemical Fluid Dynamics*, Science Publishing, Beijing (1986).

Zhou, L. X., and X. Q. Huang, "Prediction of Confined Turbulent Gas-Particle Jet by an Energy Equation Model of Particle Turbulence," *Sci. China (Ser. A)*, **33**, 428 (1990).

Manuscript received Mar. 3, 2000, and revision received Aug. 8, 2000.